Elucidating the Active Sites for CO_2 Electroreduction on Ligand-protected Au_{25} Nanoclusters

Journal:	*Catalysis Science & Technology*
Manuscript ID	CY-ART-05-2018-001099.R1
Article Type:	Paper
Date Submitted by the Author:	29-Jun-2018
Complete List of Authors:	Austin, Natalie; University of Pittsburgh, Chemical and Petroleum Engineering Zhao, Shuo; Carnegie Mellon University, Chemistry McKone, James; University of Pittsburgh, Chemical and Petroleum Engineering Jin , Rong Chao; Carnegie Mellon University, Chemistry Mpourmpakis, Giannis; University of Pittsburgh, Chemical and Petroleum Engineering

Elucidating the Active Sites for CO_2 Electroreduction on Ligand-protected Au_{25} Nanoclusters

Natalie Austin[a], Shuo Zhao[b], James R. McKone[a], Rongchao Jin[b] and Giannis Mpourmpakis[a,*]

a. Department of Chemical Engineering, University of Pittsburgh, Pittsburgh, PA 15261, USA
b. Department of Chemistry, Carnegie Mellon University, Pittsburgh, PA 15213, USA

Abstract

Using Density Functional Theory (DFT) calculations, we investigated the electrochemical reduction of CO_2 and the competing H_2 evolution reaction on ligand-protected Au_{25} nanoclusters (NCs) of different charge states, $Au_{25}(SR)_{18}^{q}$ (q = -1, 0, +1). Our results showed that regardless of charge state, CO_2 electroreduction over $Au_{25}(SR)_{18}^{q}$ NCs was not feasible because of the extreme endothermicity to stabilize the carboxyl (COOH) intermediate. When we accounted for the removal of a ligand (both -SR and -R) from $Au_{25}(SR)_{18}^{q}$ under electrochemical conditions, surprisingly we found that this is a thermodynamically feasible process at the experimentally applied potentials with the generated surface sites becoming active centers for electrocatalysis. In every case, the negatively charged NCs, losing a ligand from their surface during electrochemical conditions, were found to significantly stabilize the COOH intermediate, resulting in dramatically enhanced CO_2 reduction. The generated sites for CO_2 reduction were also found to be active for H_2 evolution, which agrees with experimental observations that these two processes compete. Interestingly, we found that the removal of an -R ligand from the negatively charged NC, resulted in a catalyst that was both active and selective for CO_2 reduction. This work highlights the importance of both the overall charge state and generation of catalytically active surface sites on ligand-protected NCs, while elucidating the CO_2 electroreduction mechanisms. Overall, our work rationalizes a series of experimental observations and demonstrates pathways to convert a very stable and catalytically inactive NC to an active electrocatalyst.

Keywords
Density Functional Theory, gold, electrochemistry, catalysis, renewable energy

*corresponding author email: gmpourmp@pitt.edu

Introduction

Growing fossil fuel consumption to meet energy demands has led to rising CO_2 emissions, which could have detrimental effects on the environment if left unmitigated.[1] There is an emerging interest in electrocatalysis as a route to reduce CO_2 emissions by sustainably converting CO_2 to useful chemicals and fuels.[2-6] Electrochemical conditions are advantageous for this reaction because applied potentials can be used to drive the reduction at ambient pressures and temperatures, and the electricity required to reduce CO_2 can be acquired from renewable resources such as wind and solar power.[7-11] Presently, the challenge with reducing CO_2 electrocatalytically is that it is not industrially feasible due to the highly reducing potentials required to obtain desired products such as hydrocarbons and CO.[7, 12, 13] Additionally, at these extreme potentials, there is low selectivity for desired products due to the competing H_2 evolution reaction.[8, 14] Therefore, there is continued interest in the design of active catalysts that promote CO_2 reduction at modest potentials while minimizing hydrogen evolution.

Experimental work by Hori et al. demonstrated that bulk Au electrodes can successfully reduce CO_2 to CO.[13, 15] Additional studies have shown that nanosized Au electrodes are more active than bulk Au electrodes.[16-18] The enhanced activity of Au nanoparticles (NPs) has been attributed to catalyst properties such as high surface area and increased presence of low-coordinated sites that strongly bind reaction intermediates.[17, 19-21] Mistry et al. investigated CO_2 reduction on Au NPs 1.1 nm to 7.7 nm in size. The authors identified that NPs below 5 nm were significantly more active than bulk Au whereas, NPs larger than 5 nm were comparably active to bulk Au. The activity of the Au NPs less than 5 nm in size was attributed to the presence of low-coordinated sites such as corners and edges. Interestingly, the catalytically more active and smaller NPs (< 5 nm) were more selective towards H_2.[16] Hall et al. showed that porous Au film thickness (ranging from 0.5 to 2.7 μm) can also influence CO_2 reduction selectivity.[22] The authors observed a suppression in hydrogen evolution with increase in film thickness, leading to increased selectivity towards CO. Thus, in addition to the presence of low-coordinated sites, mass transport effects could also play a role in resulting activity and selectivity of Au NPs for the CO_2 reduction reaction.

In contrast to polydisperse Au NPs, atomically precise Au nanoclusters (NCs), stabilized by organic ligands, exhibit well-defined structure which make them attractive for catalytic applications.[23, 24] However, the presence of ligands can also limit the accessibility of reactants to Au sites resulting in reduced catalyst activity.[25-27] Despite this, Kauffman et al., has observed enhanced catalytic activity of ligand-protected NCs compared to unprotected NPs at reducing potentials as small as -0.193 V.[18] Specifically, the authors compared the activity of a fully ligand-protected $Au_{25}(SC_2H_4Ph)_{18}^-$ NC, about 1 nm in size, to unprotected (metallic) 2 nm and 5 nm Au NPs, and bulk Au. Despite the small size of the $Au_{25}(SC_2H_4Ph)_{18}^-$ NC, contrary to Mistry et al.[16], the NC was more selective towards CO than the NPs and bulk Au. In addition, the $Au_{25}(SC_2H_4Ph)_{18}^-$ NC produced peak CO production at -1.0 V *vs* RHE, at a rate 7-700 times higher

than on the NPs and bulk Au. This suggests that the ligands designed to stabilize these Au NCs have an effect in the selective reduction of CO_2 to CO. Despite the negative potentials applied, a retention of the optical spectra before and after CO_2 reduction suggests that the $Au_{25}(SC_2H_4Ph)_{18}^-$ NC did not change size, and that the S-Au-S-Au-S bonding motif in the cluster shell was majorly retained. The potential scalability and long-term performance of electroreduction of CO_2 over the $Au_{25}(SC_2H_4Ph)_{18}^-$ NC has also been investigated.[28] Under realistic on-demand catalyst usage, CO selectivities and Faradaic efficiencies greater than 90%, were achieved through both potentiostat-controlled and renewable solar powered electrolysis. Thus, these ligand-protected Au NCs appear to be attractive electrocatalysts for feasible conversion of CO_2.

Theoretical methods combined with experiments can be used to provide atomic level insight into the catalyst properties that influence CO_2 reduction activity over Au_{25} NCs. For instance, Kauffman et al. assessed CO_2 reduction on fully ligand-protected $Au_{25}(SR)_{18}^q$ NCs in three different charge states (q= -1, 0, +1) using DFT calculations and experiments, wherein thiolate ligands were simulated with methylthiols in calculations.[29] The negatively charged NC was able to produce more CO from CO_2 reduction than the neutral and positive NCs between -0.7 V and -1.3 V *vs* RHE. The activity of $Au_{25}(SR)_{18}^-$ for CO_2 reduction was computationally attributed to the stabilization of co-adsorbed CO_2 and H^+ reactants more favorably than on $Au_{25}(SCH_3)_{18}^q$ (q= 0, +1). Such a stabilization is expected due to the electrostatic interactions between the negatively charged NC and the proton. The presence of ligand-removed NCs, due to the very negative potentials applied, was not considered in this work, neither the detailed reaction path. In a latter study, Alfonso et al. used Density Functional Theory (DFT) to investigate CO_2 reduction to CO on fully ligand-protected $Au_{25}(SCH_3)_{18}^-$ and partially ligand-removed $Au_{25}(SCH_3)_{17}^-$.[30] The authors identified that the COOH species, an important intermediate in CO_2 reduction, was more stabilized on $Au_{25}(SCH_3)_{17}^-$ (ΔG[*COOH]: 0.34 eV) than on $Au_{25}(SCH_3)_{18}^-$ (ΔG[*COOH]: 2.04 eV). The stabilization of the COOH intermediate, was attributed to its interaction with exposed Au atoms from the thiol ligand-removed site.[30] The investigation of ligand-removed $Au_{25}(SCH_3)_{17}^-$ was supported using work by Wu et al. in which the authors observed an enhancement in CO conversion over the $Au_{25}(SC_2H_4Ph)_{18}$ NC when thiol-based ligands were removed from the NC.[27] In our very recent study on the CO_2 electroreduction on sphere and rod-like ligand-protected Au NCs, we computationally showed that ligand removal can occur under electrochemical conditions and the generated sites exhibited CO_2 electoreduction trends that were observed in experiments.[31]

Results to date illustrate that there is no consensus on the identity of active sites on ligand-protected Au nanocatalysts. Some studies have proposed that under reaction conditions these catalysts remain fully ligand-protected[18, 29, 32-34] while others have stated that some ligand removal is necessary for activity to be observed[25, 27, 31, 35-39]. Additionally, there are competing claims on whether Au nanocatalysts are more selective towards CO[18, 28, 40] or H_2[16, 41] under CO_2 reduction conditions. This lack of agreement on the selectivity of Au nanocatalysts, in addition to the elusive active sites under electrocatalytic conditions, make it very difficult to identify chemical strategies

for the design and synthesis of thiolated Au NCs that efficiently reduce CO_2. Theoretical studies can give valuable insights into the reaction mechanisms and reveal active catalytic sites, but there are presently very few studies that have investigated the CO_2 reduction behavior on these ligand-protected NCs.[18, 29-31]

Herein, we report a systematic analysis of how the NC charge state and ligand-removal concertedly influence the reaction energetics of the CO_2 reduction and H_2 evolution reactions, by using DFT calculations. This work elucidates the active sites on the NC catalyst surface for CO_2 reduction and provides insight into the mechanisms of their generation that would lead to the design of more efficient CO_2 electroreduction catalysts.

Computational methods

DFT calculations in this study were carried out using the PBE[42] functional and the double-ζ plus polarization (DZVP) basis set[43] with a 500 Ry cutoff in combination with the Goedecker, Teter, and Hutter (GTH) pseudopotentials[44], as implemented in the computational package CP2K[45]. This combination of DFT parameters (functional, pseudopotentials, and basis set) has been successfully used to investigate reaction energetics on Au-based catalysts.[46-50] The initial geometries of the NCs were generated from experimentally-derived crystallographic data of the $Au_{25}(SEthPh)_{18}^-$ NC.[51] The ligands of the Au_{25} NC were represented by methylthiolate groups ($-SCH_3$) generating the $Au_{25}(SCH_3)_{18}$ NC. Simplification of the ligands, from $-SC_2H_4Ph$ to $-SCH_3$, is a typical approach used to reduce computational cost while maintaining the structural integrity of the NCs.[18, 29, 30, 35, 52] As shown in Figure 1, the $Au_{25}(SCH_3)_{18}^q$ NC is composed of a Au_{13} icosahedral core protected

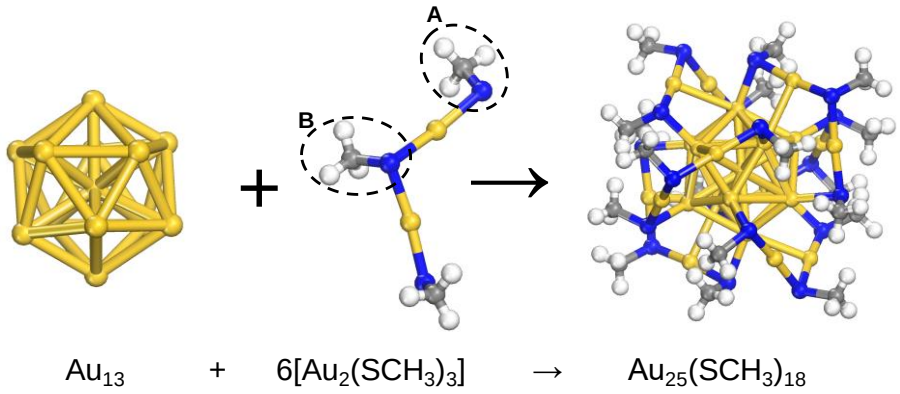

Figure 1. Schematic of the fully-ligand protected $Au_{25}(SCH_3)_{18}$ NC. The system is composed of a Au_{13} icosahedral core protected by a shell network of six $Au_2(SR)_3$ units. The Au, S, C, and H atoms are colored yellow, blue, grey, and white, respectively. The labels "A" and "B" on the $Au_2(SCH_3)_3$ shell network represent the two distinct types of coordinated sulfur in the NC shell.

by a shell network of six $Au_2(SCH_3)_3$ units. The geometries of the NCs were optimized in a 30 x 30 x 30 $Å^3$ non-periodic cell until the forces were less than 0.02 eV $Å^{-1}$. All systems with an even number of electrons had a singlet multiplicity and all systems with an odd number of electrons in

this study had a doublet multiplicity (see supporting information Table S1 for more details). The energetics for ligand removal, CO_2 reduction, and H_2 evolution were calculated using thermodynamic methods where the zero-point energy (ZPE), heat capacity (C_P), and entropic (TS) terms were added to the electronic energy (E) as follows: $\Delta G=\Delta E+\Delta ZPE+\int C_P dT-TS$. Additionally, the computational hydrogen electrode model (CHE)[12, 53] was applied to represent the free energy of a proton (H^+) and electron (e^-) pair in reduction reactions and thereby, calibrate the calculated free energy on an electrochemical scale. Thus, the total free energy for a proton-electron pair with an applied potential (U) is defined as $G(H^+ + e^-) = G(½\ H_2)-neU$ where n is the number of electrons transferred and e is the electronic charge. Gas phase corrections as calculated by Peterson et al., were also applied to the electronic energies of the gaseous molecules.[12] For the free energies of the adsorbates the vibrational components of the heat capacity and entropic terms were considered. The vibrational modes of the adsorbates were determined by keeping the optimized NC fixed and computing the frequencies of the adsorbate within the harmonic oscillator approximation. This approach has been successfully applied using DFT in electrocatalysis[19, 30, 54, 55], including $Au_{25}(SCH_3)_{18}$. The computationally predicted limiting potential (U_L)[12, 56] was calculated as the applied potential required for the rate determining step, to become thermoneutral ($\Delta G = 0$).

The Au_{25}^q NC which has been stably synthesized in multiple charge states (q = -1, 0, +1)[57-59] has also been used for catalysis in each of the charge states.[29] In the supporting information (Table S2) we assess the relative stability of the Au_{25} NC in relation to the charge states using adiabatic electron affinity (AEA, $Au_{25}(SCH_3)_x^0 + e^- \rightarrow Au_{25}(SCH_3)_x^-$) and adiabatic ionization potential (AIP, $Au_{25}(SCH_3)_x^0 \rightarrow Au_{25}(SCH_3)_x^+ + e^-$).[60, 61] Studies have also suggested that under reaction conditions, the Au_{25} NC can partially lose ligands.[27, 30] Therefore we calculate the energy required to remove ligands from the $Au_{25}(SCH_3)_{18}$ NC. We initially focus on the removal of –SR (-SCH_3) from the 6[$Au_2(SCH_3)_3$] shell of the fully ligand-protected NC in each different charge state. The removal of a -SR ligand would expose an Au atom and enable interaction with adsorbates. However, theoretical studies on CO_2 reduction on Ni-Fe-S Cubanes[54] and MoS_2[62] catalysts have shown that the COOH intermediate can be stabilized more favorably on the S atoms of the catalysts compared to other available sites. Thus, we also considered removal of –R (-CH_3) from the Au_{25} NCs to expose an S atom to the reaction intermediates for CO_2 reduction to CO.

The ΔG for ligand removal of -SR from $Au_{25}(SCH_3)_{18}$ was calculated as an electrochemical reduction step, using Equation 1, which was derived according to the following reduction reaction: $Au_{25}(SCH_3)_{18}^q + H^+ + e^- \rightarrow HSCH_3 + Au_{25}(SCH_3)_{17}^q$.

$$\Delta G_{methylthiol\text{-}removal} = G[Au_{25}(SCH_3)_{17}]^q + G[HSCH_3] - G[Au_{25}(SCH_3)_{18}]^q - ½\ G[H_2] + neU \quad (1)$$

Where $G[Au_{25}(SCH_3)_{17}]$, $G[HSCH_3]$, $G[Au_{25}(SCH_3)_{18}]$, and $G[H_2]$ are the gas phase free energies of the isolated NC with a removed thiol, the $HSCH_3$ molecule, the fully ligand-protected NC, and the H_2 molecule, respectively. The ΔG for removal of -R was calculated in the same manner as for -SR with $G[Au_{25}(SCH_3)_{17}]^q$ and $G[HSCH_3]$ in Equation 1 being replaced by $G[Au_{25}S(SCH_3)_{17}]^q$

and G[CH_4], respectively. All vibrational modes were considered in the analysis of free energies of ligand removal. An overview of the potential states of the Au_{25}^q NC under reaction conditions that we consider in this study are shown in Figure 2 (shown for $–SCH_3$ removal).

Prior studies have suggested[12, 17, 30] that CO_2 reduction and hydrogen evolution can take place through the following steps:

$$CO_2 + H^+ + e^- + * \rightarrow *COOH \quad (2)$$
$$*COOH + H^+ + e^- \rightarrow *CO + H_2O(l) \quad (3)$$
$$*CO \rightarrow CO(g) + * \quad (4)$$

$$H^+ + e^- + * \rightarrow *H \quad (5)$$
$$*H + H^+ + e^- + * \rightarrow H_2(g) + * \quad (6)$$

An example for determining reaction energetics using the first step of CO_2 reduction on the NCs (2), is calculated as follows:

$$\Delta G_{*COOH} = G[COOH*] - G[NC] - G[CO_2] - \tfrac{1}{2} G[H_2] + neU \quad (7)$$

Where G[COOH*], G[NC], G[CO_2], G[H_2] are the gas phase free energies of the COOH adsorbed on a NC, the NC, the CO_2 molecule, and the H_2 molecule, respectively. In the supporting information (Figure S1) we also assessed CO_2 adsorption on the NCs and observed only physisorbed CO_2 as previously reported[18].

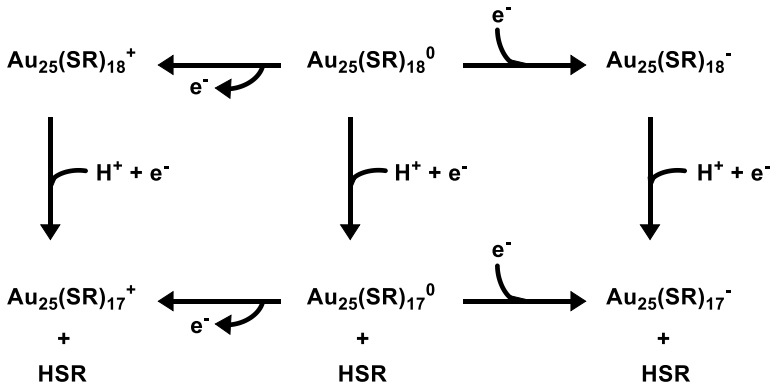

Figure 2. A cycle which illustrates potential states of the Au_{25} NC under reaction conditions. The top and bottom rows, show electron transfer to form the fully ligand-protected and partially ligand removed NCs in each charge state, respectively. The vertical steps indicate ligand removal from $Au_{25}(SR)_{18}^q$ to form $Au_{25}(SR)_{17}^q$.

Results

DFT geometry optimizations illustrated that the final structures of the fully ligand-protected $Au_{25}(SR)_{18}^q$ (q = -1, 0, +1) NCs are nearly structurally identical to the experimental crystal

structure[29, 57, 59, 63]. The calculated free energy diagrams for CO_2 reduction and H_2 evolution on the fully ligand-protected $Au_{25}(SCH_3)^q$ NCs (q= -1, 0, +1), at U=0 V (solid lines) are shown in Figure 3. The ΔG values of the reactions were also evaluated at an applied potential of -1.0 V *vs*

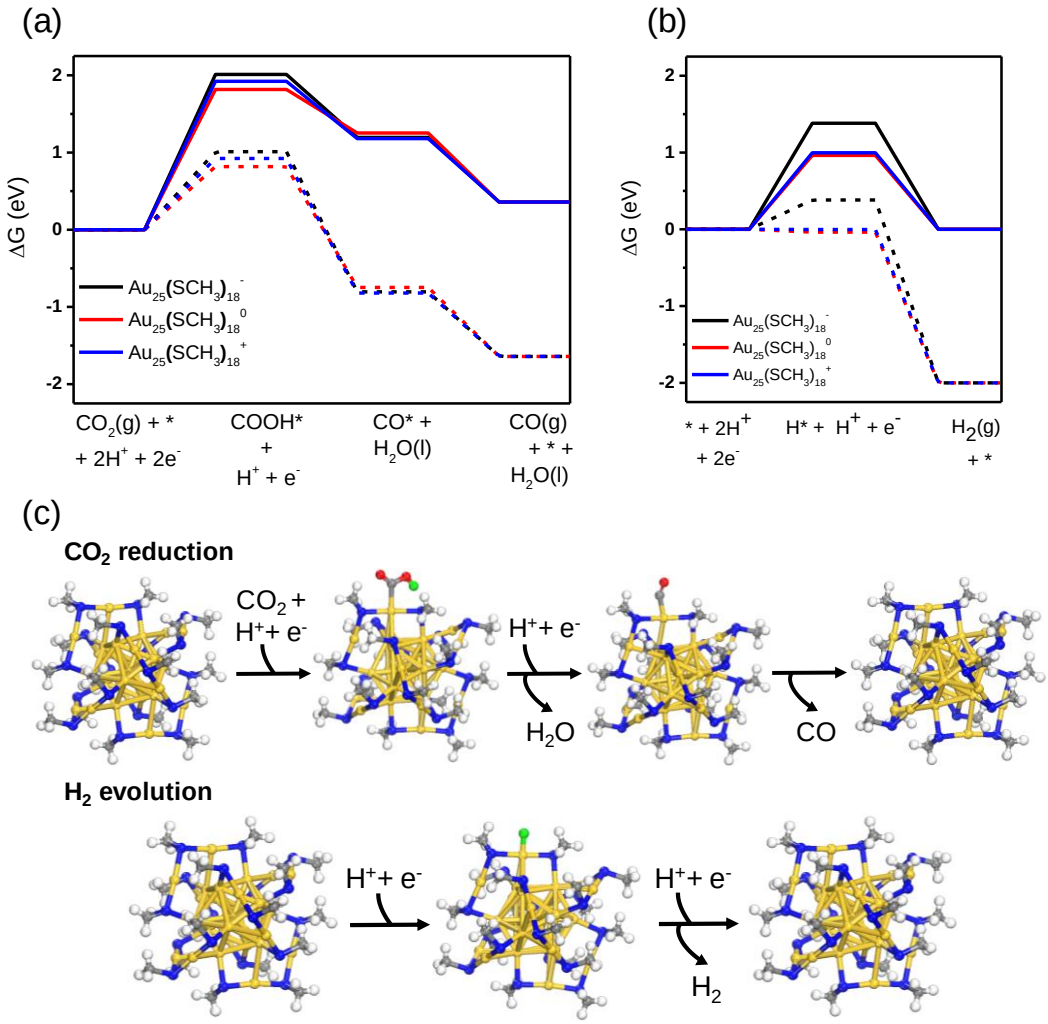

Figure 3. Free energy diagrams (ΔG) for the (a) reduction of CO_2 to CO and (b) hydrogen evolution on the fully ligand-protected $Au_{25}(SCH_3)_{18}^q$ (q= -1, 0, +1) NCs. The black, red, and blue lines represent the energy diagrams generated using a NC in the -1, 0, and +1 charge states, respectively. The solid lines illustrate the energy diagrams at U = 0 V, while the dashed lines represent the energy diagrams at an applied potential of U = -1.0 V. (c) Illustrations of the CO_2 reduction and the hydrogen evolution reactions. The Au, S, C, and O, atoms are colored yellow, blue, grey, and red, respectively. The H atoms are white, except for H on the carboxyl (in CO_2 reduction) and the adsorbed H (in hydrogen evolution) which are colored lime green for clarity.

RHE (U = -1.0 V, dashed lines in Figure 3), the potential at which peak production of CO was observed in experimental studies on the NCs.[18, 28] As shown in Figure 3a, CO_2 reduction to CO on the fully ligand-protected NCs $Au_{25}(SCH_3)_{18}$ in each charge state, appears to be unfavorable due to the largely endergonic step for COOH stabilization (ΔG > 1.82 eV) . The observed unfavorable ΔG (*COOH), agrees with previous computational observations by Alfonso et al., for CO_2 reduction on the $Au_{25}(SCH_3)_{18}^-$ NC.[30] Although for the hydrogen evolution reaction at U=0 V, the H adsorption step is also endergonic (Figure 3b), the ΔG for the H adsorption (Equation 5) is more

favorable than the COOH adsorption (Equation 2). Furthermore, at U = -1.0 V, the hydrogen evolution reaction becomes exergonic on the $Au_{25}(SCH_3)_{18}^{q}$ (q = 0, +1) NCs. Overall, the large positive ΔG values for CO_2 reduction on the fully ligand-protected NCs suggest that the production of CO is not feasible on these NCs. Thus, we focused on partially ligand-removed NCs, which have been experimentally shown to be active catalysts.[27, 35-39]

Figure 4a illustrates partial ligand removal from the $Au_{25}(SCH_3)_{18}$ NC via a reduction reaction. We focus on removing one -SCH_3 ligand, connected to a core Au atom of the NC (labeled in Figure 1 as site "A" and also shown in Figure 4a), as has been done in previous studies[30]. It should be noted that removing -SCH_3 from site "A" in Figure 1 is more energetically favorable than from site "B" (see Figure S2 in the supporting information). In the resulting partially ligand-removed $Au_{25}(SCH_3)_{17}$ NC, the Au atom of the shell, which was previously bound to the removed -SCH_3 ligand, is now connected to an Au atom of the core. According to our geometry optimization calculations, aside from the site where the -SCH_3 ligand was removed, the $Au_{25}(SCH_3)_{17}^{q}$ NCs remain geometrically similar to the $Au_{25}(SCH_3)_{18}^{q}$ NC. To assess the ability of the $Au_{25}(SCH_3)_{18}^{q}$ NCs to release a -SCH_3 ligand, we calculated the ΔG for the electrochemical step of $Au_{25}(SCH_3)_{17}^{q}$ formation from $Au_{25}(SCH_3)_{18}^{q}$ as shown in Figure 4b. The observed trend in ΔG for removing a ligand from $Au_{25}(SCH_3)_{18}^{q}$ at U = 0 V and -1.0 V is as follows (from most favorable to least favorable): $Au_{25}(SCH_3)_{18}^{0}$ < $Au_{25}(SCH_3)_{18}^{+}$ < $Au_{25}(SCH_3)_{18}^{-}$. This trend follows the order of increasing stability of the fully ligand-protected NCs as depicted on the increasing HOMO – LUMO gaps, calculated by Akola et al.[64] At U = 0 V the formation of the partially ligand-removed $Au_{25}(SCH_3)_{17}^{q}$ NCs is less endergonic than the COOH adsorption on the fully ligand-protected $Au_{25}(SCH_3)_{18}^{q}$ NCs. Interestingly, at U = -1.0 V, the ΔG for $Au_{25}(SCH_3)_{17}$ formation becomes exergonic in each charge state, as shown by the dashed lines in Figure 4b. Thus, under reaction

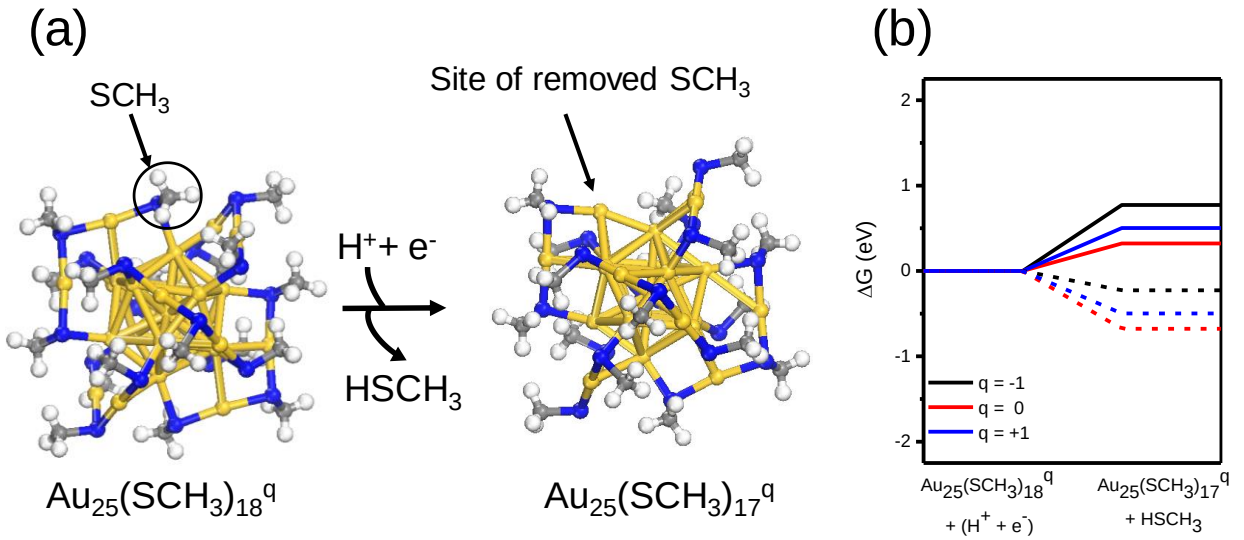

Figure 4. (a) Schematic for the reduction of the fully ligand-protected NCs ($Au_{25}(SCH_3)_{18}^{q}$) to partially ligand-removed $Au_{25}(SCH_3)_{17}^{q}$. The color code is as shown in Figure 3. (b) Free energy diagram for removing one -SCH_3 from the NC. As described in Figure 3, the colored, solid, and dashed lines represent the different charge states and energetics at U = 0 V and at U = -1.0 V, respectively.

conditions (-1.0 V *vs.* RHE) calculations clearly predict the formation of partially ligand-removed catalysts.

Following the observation of exergonic ΔG for $Au_{25}(SCH_3)_{17}^{q}$ formation at U = -1.0 V, we assessed CO_2 reduction and H_2 evolution on the $Au_{25}(SCH_3)_{17}^{q}$ NCs (q = -1, 0, +1). As shown in Figure 5a, we found that the partially ligand-removed NCs better stabilized the COOH intermediate (ΔG < 1.42 eV) relative to the fully ligand-protected NCs (ΔG > 1.82 eV). Thus, in each charge state the

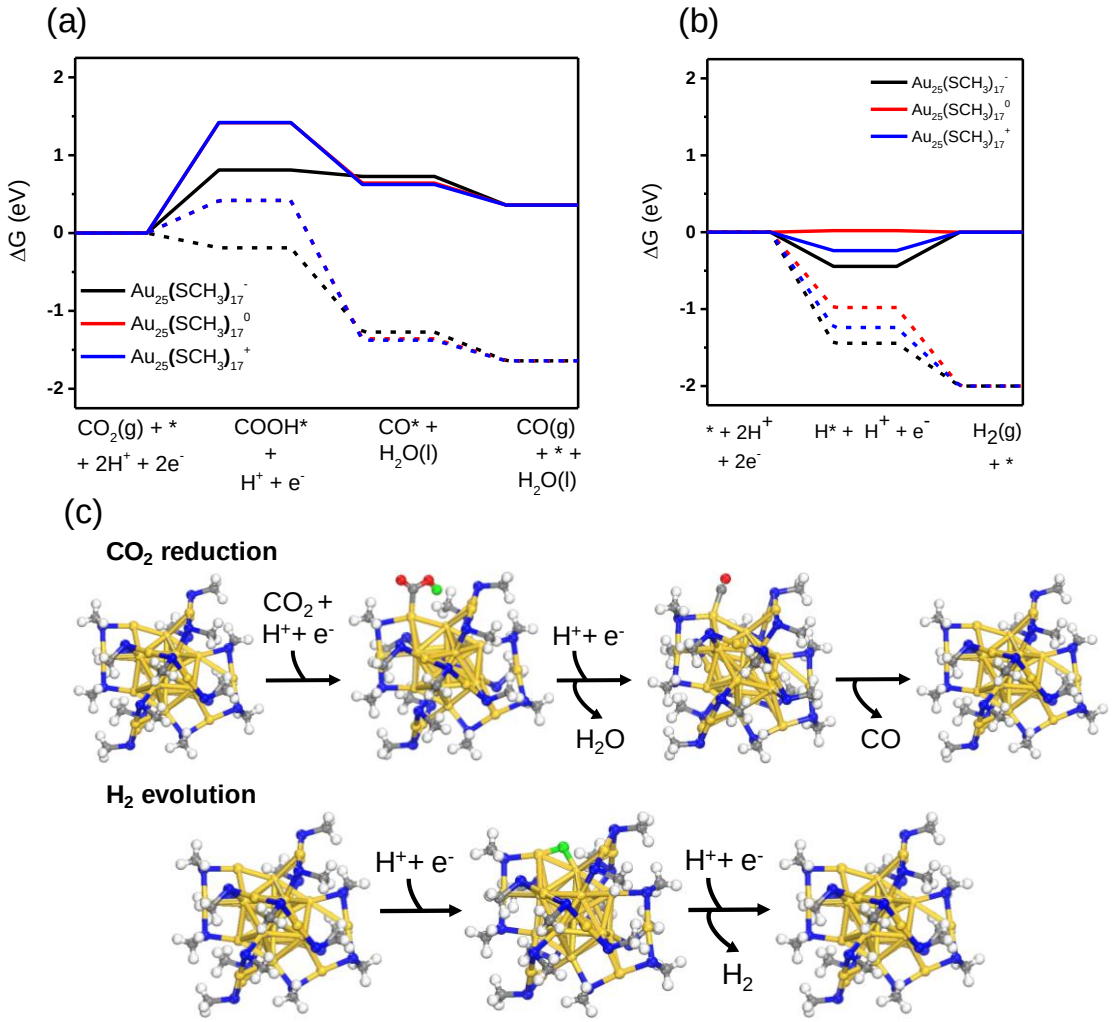

Figure 5. Free energy diagrams (ΔG) for the (a) reduction of CO_2 to CO and the (b) hydrogen evolution reaction on the $Au_{25}(SCH_3)_{17}^{q}$ (q= -1, 0, +1) NCs (with a ligand removed). (c) Illustrations of CO_2 reduction and H_2 evolution reaction steps. The color code for the diagrams is as described in Figure 3.

presence of ligand-removed sites on the NCs enhances COOH surface stabilization compared to the fully ligand-protected NCs. The lower ΔG(*COOH) observed on the $Au_{25}(SCH_3)_{17}^{q}$ NCs suggests that ligand removal is important for the Au NCs to become active, as highly endergonic free energies were observed on the fully ligand-protected NCs even with an applied potential (U = -1.0 V). The $Au_{25}(SCH_3)_{17}^{-}$ NC had the least endergonic ΔG(*COOH) compared to

$Au_{25}(SCH_3)_{17}^{q}$ (q= 0, +1) at U = 0 V, which is conceptually consistent with the Lewis acidity of CO_2. Thus, we would expect the partially ligand-removed NCs to be most active in a negative charge state. Given the exergonic ΔG(*H) shown in Figure 5b, we would also expect competition with H_2 evolution on partially ligand-removed NCs. It should be noted that adsorbate interactions can be influenced by solvation.[56] Thus, in the supporting information (Figure S3) we assessed the H_2O solvent effect on CO_2 reduction and H_2 evolution energetics on the $Au_{25}(SCH_3)_{17}^{-}$ NC. The

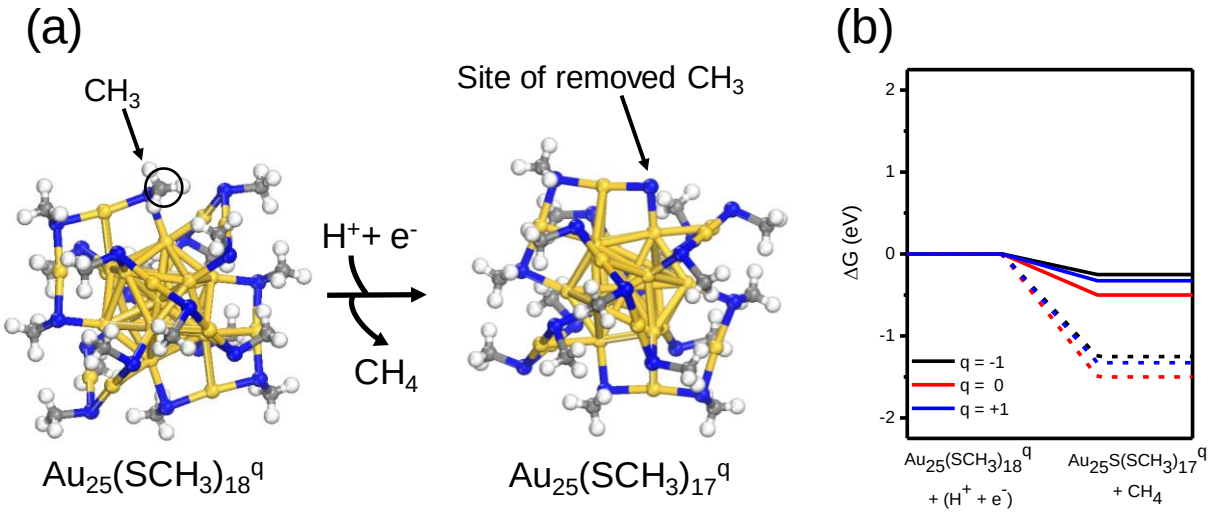

Figure 6. (a) Schematic for the reduction of the fully ligand-protected NC ($Au_{25}(SCH_3)_{18}^{q}$) to one with -CH_3 removed, $Au_{25}S(SCH_3)_{17}^{q}$. The color code is as shown in Figure 3. (b) Free energy diagram for removing one -CH_3 from the NC. As described in Figure 3, the colored, solid, and dashed lines, represent the charge states, the energetics at U = 0 V and at U = -1.0 V, respectively.

results showed an enhancement in stabilizing the COOH intermediate in the presence of H_2O. Additionally, the trends observed without solvation (i.e. competition with H_2 evolution), remained in the solvated case studied.

Having shown that the ligand removal on the NCs can generate active sites for CO_2 electroreduction and knowing that catalysts with surface sulfur atoms, such as Ni-Fe-S Cubanes[54] and MoS_2[62], stabilize the COOH intermediate in CO_2 reduction, we investigated the removal of -CH_3 from the $Au_{25}(SCH_3)_{18}$ NC to generate a surface sulfur site instead of a bare Au site (Figure 6a). Similarly, to -SCH_3 removal, we focus on removing -CH_3 from site "A" as indicated in Figure 1, in each charge state of the Au_{25} NC. The observed trend for removing a -CH_3 from $Au_{25}(SCH_3)_{18}^{q}$ at U = 0 V and -1.0 V is the same as removing -SCH_3 from $Au_{25}(SCH_3)_{18}^{q}$: $Au_{25}(SCH_3)_{18}^{0}$ < $Au_{25}(SCH_3)_{18}^{+}$ < $Au_{25}(SCH_3)_{18}^{-}$ (from most favorable to least favorable). Remarkably, unlike the endergonic ΔG observed for -SCH_3 removal at U = 0 V, the ΔG for -CH_3 removal is exergonic in each charge state. Thus, under reaction conditions (-1.0 V *vs.* RHE) calculations predict that bare Au sites (due to -SCH_3 removal) and S sites (due to -CH_3 removal) may coexist. However, we note that we have not assessed here the free energies for ligand removal associated with an experimentally utilized ligand (i.e. -SC_2H_4Ph) due to computational constraints. However, in the supporting information (Figure S4) we present an energy analysis comparing -

SC_2H_4Ph removal to -C_2H_4Ph removal in the negatively charged state of the Au_{25} NC. These results indicate that under reaction conditions the formation of the partially-ligand removed NCs is still plausible.

Due to the preferable ΔG(*COOH) on $Au_{25}(SCH_3)_{17}^-$ relative to $Au_{25}(SCH_3)_{17}^q$ (q= 0, +1), we examine CO_2 reduction and H_2 evolution on the $Au_{25}S(SCH_3)_{17}^-$ NC (-CH_3 removed) and compare the energetics to the $Au_{25}(SCH_3)_{17}^-$ NC (-SCH_3 removed). As shown in Figure 7a, we found that $Au_{25}S(SCH_3)_{17}^-$ stabilizes COOH more favorably (ΔG(*COOH) = 0.33 eV) relative to $Au_{25}(SCH_3)_{17}^-$ NC (ΔG(*COOH) = 0.81 eV. This enhanced COOH adsorption could be attributed to the larger negative charge on the exposed S site of the $Au_{25}S(SCH_3)_{17}^-$ compared to the exposed Au site of the $Au_{25}(SCH_3)_{17}^-$ NC (see supporting information Figure S5). In addition, the exposed S site of the $Au_{25}S(SCH_3)_{17}^-$ NC contributes to increased electron density near the Fermi level of

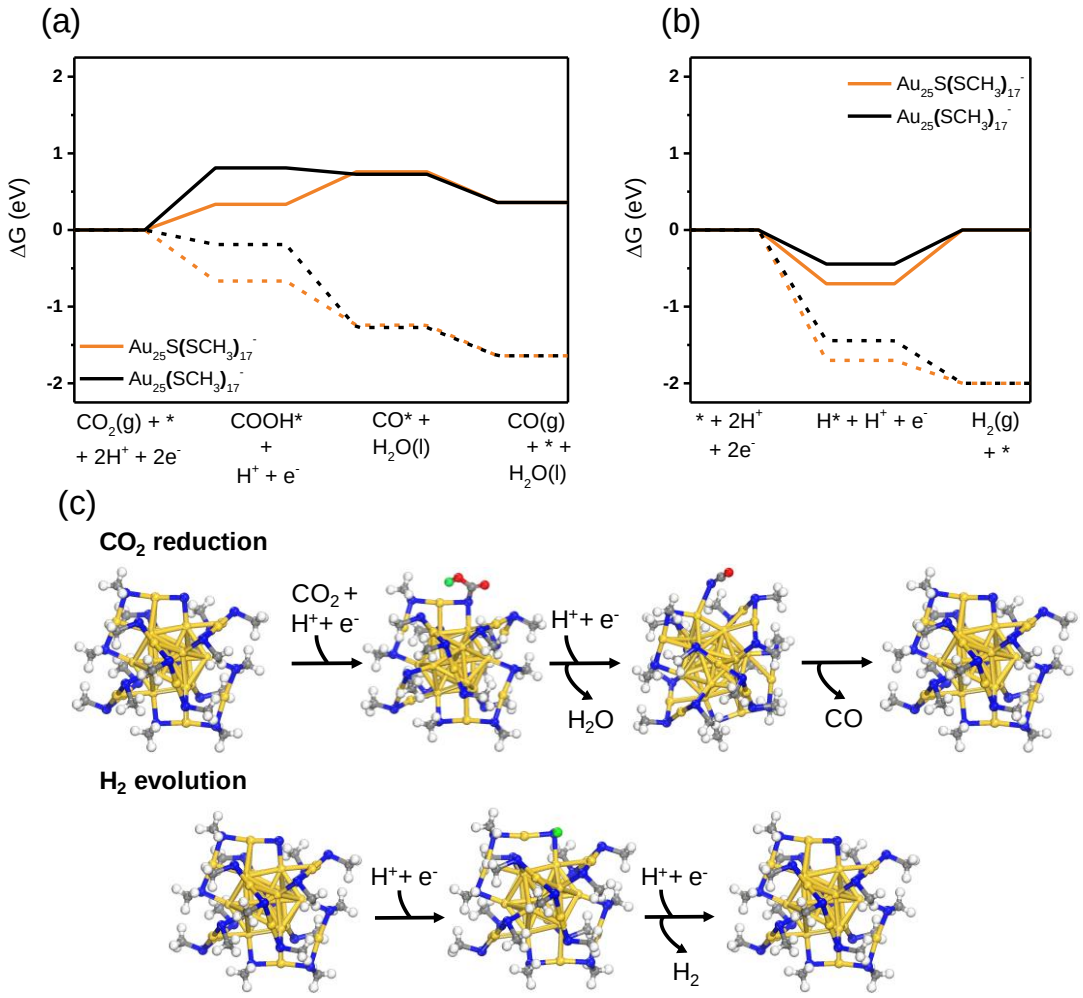

Figure 7. Free energy diagrams (ΔG) for the (a) reduction of CO_2 to CO and the (b) hydrogen evolution on the -CH_3 removed $Au_{25}S(SCH_3)_{17}^-$ NC and on the -SCH_3 removed $Au_{25}(SCH_3)_{17}^-$ NC. The orange and black lines represent the energy diagrams for the $Au_{25}S(SCH_3)_{17}^-$ and $Au_{25}(SCH_3)_{17}^-$ NCs, respectively. The solid lines illustrate the energy diagrams at U = 0 V, while the dashed lines represent the energy diagrams at an applied potential of U = -1.0 V. The color code for (c) the illustrations of CO_2 reduction and H_2 evolution are as described in Figure 3.

the $Au_{25}S(SCH_3)_{17}^-$ NC compared to the fully protected $Au_{25}(SCH_3)_{18}^-$, which in turn contributes to the reactivity of the NC (see supporting information Figure S6). In Figure 7b, we also observe that H adsorption at U = 0 V is more exergonic on $Au_{25}S(SCH_3)_{17}^-$ than on $Au_{25}(SCH_3)_{17}^-$. This indicates that H_2 evolution would compete with CO_2 reduction on $Au_{25}S(SCH_3)_{17}^-$ NCs.

Determining the selectivity between CO_2 reduction and hydrogen evolution would typically require an in depth kinetic analysis. However, to give a qualitative estimate of the selectivity we determine the difference between the limiting potentials for CO_2 reduction and H_2 evolution ($U_L(CO_2)$ - $U_L(H_2)$).[62, 65, 66] The more positive $U_L(CO_2)$ - $U_L(H_2)$ corresponds to a higher selectivity towards CO_2 reduction relative to the set of NCs. As shown in Table 1, on the $Au_{25}(SCH_3)_{18}^q$ and $Au_{25}(SCH_3)_{17}^q$ NCs, the limiting step which determines $U_L(CO_2)$ is the COOH formation step. However, on the $Au_{25}S(SCH_3)_{17}^-$ NC, the limiting step is CO (and H_2O) formation, which results in the smallest $|U_L(CO_2)|$ amongst all of the nanoclusters in this study. H adsorption is the limiting step that determines $U_L(H_2)$ on the $Au_{25}(SCH_3)_{18}^q$ and the $Au_{25}(SCH_3)_{17}^0$ NCs, while the formation of $H_2(g)$ is the limiting step responsible for $U_L(H_2)$ on the $Au_{25}(SCH_3)_{17}^q$ (q = +1, -1) and $Au_{25}S(SCH_3)_{17}^-$ NCs due to the exothermic H adsorption on the NCs. In Figure 8, the calculated $U_L(CO_2)$ - $U_L(H_2)$ shows that the negatively charged species, $Au_{25}(SCH_3)_{18}^-$, $Au_{25}(SCH_3)_{17}^-$, and $Au_{25}S(SCH_3)_{17}^-$ are the least selective towards H_2 production relative to the set of NCs. Although our results show that only the partially-ligand removed clusters, $Au_{25}(SCH_3)_{17}^-$ and $Au_{25}S(SCH_3)_{17}^-$, are most active for CO_2 reduction, it is only the $Au_{25}S(SCH_3)_{17}^-$ NC which is selective to CO_2 reduction over H_2 evolution (positive value of $U_L(CO_2)$ - $U_L(H_2)$) . Therefore, the exposure of S atoms, within the NCs are important to tune selectivity towards CO_2 reduction. In experiments, the conditions that control the selectivity of the Au_{25} catalyst towards CO include applied potentials, CO_2 flow rate, catalyst loading, and concentration of the electrolyte.[28, 67] These Au_{25} catalysts are also clearly active toward H_2 evolution. Shuo et al., showed that an Au_{25}/MoS_2 system enhanced the hydrogen evolution reaction activity compared to MoS_2 alone.[68] This enhanced activity was attributed to the electronic interactions at the Au-MoS_2 interface. Therefore, these Au NCs can display exceptional but different catalytic behavior depending on the chemical environment. The observed differences in catalytic behavior with changes to NC structure (fully-protected vs partially-ligand removed) shown in this study can be connected to the frontier orbitals HOMO-LUMO of the clusters (see supporting information Figure S7). As shown in Figure S7(a), the HOMO-LUMO gap of the NCs with a removed ligand becomes much smaller compared to the fully protected NC. In addition, the electron density observed on the ligand removed sites of $Au_{25}(SCH_3)_{17}^-$ and $Au_{25}S(SCH_3)_{17}^-$ becomes more localized and directional compared to $Au_{25}(SCH_3)_{18}^-$ (see Figure S7 (b)) which is important because changes in orbital localization and directionality has been shown to contribute to the reactivity of Au clusters. [69, 70]

Table 1. Limiting step and potential of the Au_{25} NCs. $H^+ + e^-$ omitted for simplicity.

	CO_2	$U_L(CO_2)$	H_2	$U_L(H_2)$
$Au_{25}(SCH_3)_{18}^-$	$CO_2 + * \rightarrow *COOH$	-2.01 V	$* \rightarrow *H$	-1.38 V
$Au_{25}(SCH_3)_{18}^0$	$CO_2 + * \rightarrow *COOH$	-1.82 V	$* \rightarrow *H$	-0.96 V
$Au_{25}(SCH_3)_{18}^+$	$CO_2 + * \rightarrow *COOH$	-1.92 V	$* \rightarrow *H$	-1.00 V
$Au_{25}(SCH_3)_{17}^-$	$CO_2 + * \rightarrow *COOH$	-0.81 V	$*H \rightarrow H_2(g) + *$	-0.44 V
$Au_{25}(SCH_3)_{17}^0$	$CO_2 + * \rightarrow *COOH$	-1.42 V	$* \rightarrow *H$	-0.02 V
$Au_{25}(SCH_3)_{17}^+$	$CO_2 + * \rightarrow *COOH$	-1.42 V	$*H \rightarrow H_2(g) + *$	-0.24 V
$Au_{25}S(SCH_3)_{17}^-$	$*COOH \rightarrow *CO + H_2O(l)$	-0.42 V	$*H \rightarrow H_2(g) + *$	-0.70 V

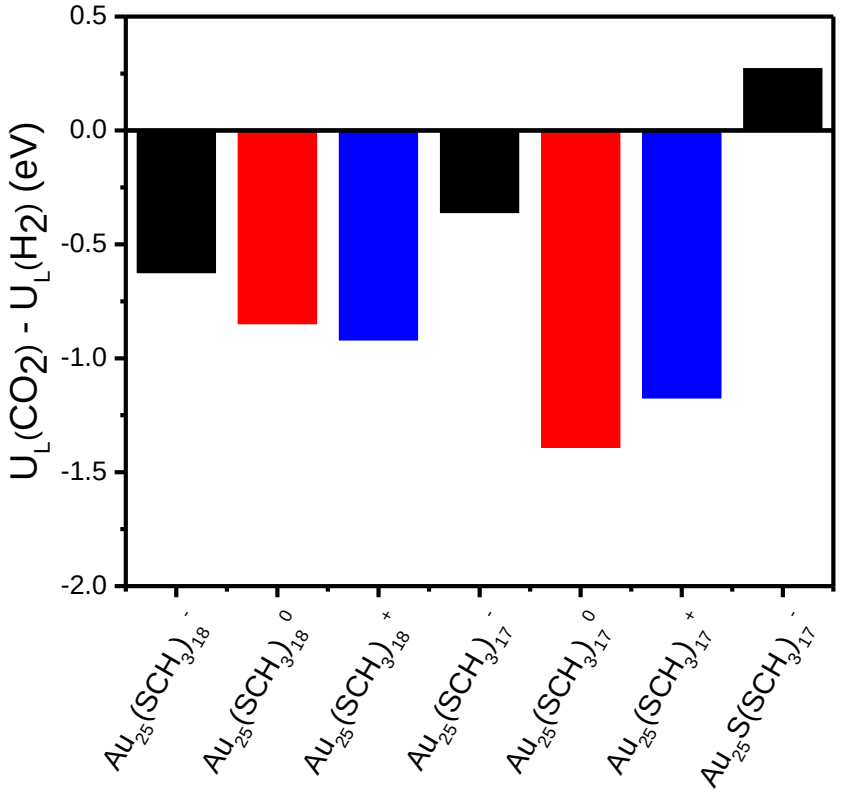

Figure 8. (a) Difference in limiting potentials of CO_2 reduction and hydrogen evolution (U_L (CO_2) - $U_L(H_2)$). The color code represents the three charge states of the Au_{25} NC (black: negative, red: neutral, blue: positive).

As a final note, although our results rationalize a series of experimental observations, they are solely based on thermodynamic viewpoints and do not take into consideration kinetic limitations in the form of activation barriers. Barriers for proton-electron transfer in CO_2 reduction to CH_4 and CH_3OH have been calculated on Pt, Cu, and Au surfaces.[71, 72] The calculated barriers for the steps relevant to this study (see Equations 2 and 3) were less than 1 eV which is surmountable under room temperature at experimentally applied potentials (U = -1.0 V). Thus, we would expect the proton-electron transfer barriers for CO_2 reduction on the Au NCs to be thermally accessible

at room temperature. Furthermore, assuming the activation energies for the proton-electron transfer steps scale with ΔG_{rxn}, as in the the Brønsted–Evans–Polanyi relationship, we would expect the lowest barriers to be observed on the ligand removed NCs.[71] In our future work, we aim to address the detailed kinetic barriers for ligand removal, which appear to be thermodynamically feasible and responsible for converting an inert NC to an active one, as well as to probe the number of ligands a NC can lose while still maintaining structural integrity.

Conclusions

In this work, we applied *ab initio* electronic structure calculations to assess CO_2 reduction and H_2 evolution on fully ligand-protected ($Au_{25}(SR)_{18}^{q}$) and partially ligand-removed (removal of -SR and -R) NCs in three charge states q = -1, 0, and +1. Our results demonstrate that regardless of charge state, the $Au_{25}(SR)_{18}^{q}$ NC is inactive for CO_2 reduction due to the relative instability of the associated COOH intermediate. On the contrary, our calculations showed that the formation of partially-ligand removed NCs, $Au_{25}(SR)_{17}^{q}$ (q = -1, 0, +1) and $Au_{25}S(SR)_{17}^{-}$, are feasible under reaction conditions. Moreover, $Au_{25}(SR)_{17}^{q}$ NCs and the $Au_{25}S(SR)_{17}^{-}$ NC stabilized the COOH intermediate more favorably than the $Au_{25}(SR)_{18}^{q}$ NCs. We therefore conclude that partially-ligand removed clusters, which expose Au and S sites, are the most active for CO_2 reduction under experimentally applied potentials. We found that hydrogen evolution likely competes with CO_2 reduction over the entire potential range of interest. By assessing selectivity, we determined that only the active $Au_{25}S(SR)_{17}^{-}$ NC would be selective towards CO_2 reduction over H_2 evolution. Overall, this work elucidates NC charge state and generation of active surface sites during electrocatalysis as responsible for the stabilization intermediates in CO_2 reduction to CO.

Acknowledgements

GM acknowledges support by the National Science Foundation (NSF, CBET-CAREER program) under Grant No. 1652694. NA acknowledges support by the NSF Graduate Research Fellowship under Grant No. 1247842. GM and NA would like to acknowledge computational support from the Center for Research Computing and the Extreme Science and Engineering Discovery Environment, which is supported by the NSF (ACI-1548562).

References

1. IPCC, *Climate Change 2013: The Physical Science Basis. Contribution of Working Group I to the Fifth Assessment Report of the Intergovernmental Panel on Climate Change*, Cambridge University Press, Cambridge, United Kingdom and New York, NY, USA, 2013.
2. J. Albo, M. Alvarez-Guerra, P. Castano and A. Irabien, *Green Chemistry*, 2015, **17**, 2304-2324.
3. K. P. Kuhl, E. R. Cave, D. N. Abram and T. F. Jaramillo, *Energy & Environmental Science*, 2012, **5**, 7050-7059.
4. A. A. Peterson and J. K. Norskov, *Journal of Physical Chemistry Letters*, 2012, **3**, 251-258.
5. C. W. Li and M. W. Kanan, *Journal of the American Chemical Society*, 2012, **134**, 7231-7234.

6. H. A. Hansen, J. B. Varley, A. A. Peterson and J. K. Norskov, *Journal of Physical Chemistry Letters*, 2013, **4**, 388-392.
7. J. L. Qiao, Y. Y. Liu, F. Hong and J. J. Zhang, *Chem. Soc. Rev.*, 2014, **43**, 631-675.
8. B. Khezri, A. C. Fisher and M. Pumera, *Journal of Materials Chemistry A*, 2017, **5**, 8230-8246.
9. E. L. Clark, C. Hahn, T. F. Jaramillo and A. T. Bell, *Journal of the American Chemical Society*, 2017, **139**, 15848-15857.
10. Gurudayal, J. Bullock, D. F. Sranko, C. M. Towle, Y. W. Lum, M. Hettick, M. C. Scott, A. Javey and J. Ager, *Energy & Environmental Science*, 2017, **10**, 2222-2230.
11. X. H. Zhou, R. Liu, K. Sun, Y. K. Chen, E. Verlage, S. A. Francis, N. S. Lewis and C. X. Xiang, *Acs Energy Letters*, 2016, **1**, 764-770.
12. A. A. Peterson, F. Abild-Pedersen, F. Studt, J. Rossmeisl and J. K. Norskov, *Energy & Environmental Science*, 2010, **3**, 1311-1315.
13. Y. Hori, *Electrochemical CO2 reduction on metal electrodes*, Springer, New York, 2008.
14. D. T. Whipple and P. J. A. Kenis, *Journal of Physical Chemistry Letters*, 2010, **1**, 3451-3458.
15. Y. Hori, K. Kikuchi and S. Suzuki, *Chem. Lett.*, 1985, DOI: 10.1246/cl.1985.1695, 1695-1698.
16. H. Mistry, R. Reske, Z. H. Zeng, Z. J. Zhao, J. Greeley, P. Strasser and B. R. Cuenya, *Journal of the American Chemical Society*, 2014, **136**, 16473-16476.
17. W. L. Zhu, R. Michalsky, O. Metin, H. F. Lv, S. J. Guo, C. J. Wright, X. L. Sun, A. A. Peterson and S. H. Sun, *Journal of the American Chemical Society*, 2013, **135**, 16833-16836.
18. D. R. Kauffman, D. Alfonso, C. Matranga, H. F. Qian and R. C. Jin, *Journal of the American Chemical Society*, 2012, **134**, 10237-10243.
19. S. Back, M. S. Yeom and Y. Jung, *ACS Catal.*, 2015, **5**, 5089-5096.
20. B. Hvolbaek, T. V. W. Janssens, B. S. Clausen, H. Falsig, C. H. Christensen and J. K. Norskov, *Nano Today*, 2007, **2**, 14-18.
21. C. Rogers, W. S. Perkins, G. Veber, T. E. Williams, R. R. Cloke and F. R. Fischer, *Journal of the American Chemical Society*, 2017, **139**, 4052-4061.
22. A. S. Hall, Y. Yoon, A. Wuttig and Y. Surendranath, *Journal of the American Chemical Society*, 2015, **137**, 14834-14837.
23. R. C. Jin, H. F. Qian, Z. K. Wu, Y. Zhu, M. Z. Zhu, A. Mohanty and N. Garg, *Journal of Physical Chemistry Letters*, 2010, **1**, 2903-2910.
24. G. Li and R. C. Jin, *Accounts Chem. Res.*, 2013, **46**, 1749-1758.
25. P. Haider, A. Urakawa, E. Schmidt and A. Baiker, *Journal of Molecular Catalysis a-Chemical*, 2009, **305**, 161-169.
26. L. D. Menard, F. T. Xu, R. G. Nuzzo and J. C. Yang, *Journal of Catalysis*, 2006, **243**, 64-73.
27. Z. L. Wu, D. E. Jiang, A. K. P. Mann, D. R. Mullins, Z. A. Qiao, L. F. Allard, C. J. Zeng, R. C. Jin and S. H. Overbury, *Journal of the American Chemical Society*, 2014, **136**, 6111-6122.
28. D. R. Kauffman, J. Thakkar, R. Siva, C. Matranga, P. R. Ohodnicki, C. J. Zeng and R. C. Jin, *Acs Applied Materials & Interfaces*, 2015, **7**, 15626-15632.
29. D. R. Kauffman, D. Alfonso, C. Matranga, P. Ohodnicki, X. Y. Deng, R. C. Siva, C. J. Zeng and R. C. Jin, *Chem. Sci.*, 2014, **5**, 3151-3157.
30. D. R. Alfonso, D. Kauffman and C. Matranga, *Journal of Chemical Physics*, 2016, **144**, 184705.
31. S. Zhao, N. Austin, M. Li, Y. Song, S. D. House, S. Bernhard, J. C. Yang, G. Mpourmpakis and R. Jin, *ACS Catal.*, 2018, DOI: 10.1021/acscatal.8b00365, 4996-5001.
32. X. T. Nie, H. F. Qian, Q. J. Ge, H. Y. Xu and R. C. Jin, *Acs Nano*, 2012, **6**, 6014-6022.
33. G. Centi, E. A. Quadrelli and S. Perathoner, *Energy & Environmental Science*, 2013, **6**, 1711-1731.
34. X. Chen and H. Hakkinen, *Journal of the American Chemical Society*, 2013, **135**, 12944-12947.
35. G. Li, H. Abroshan, Y. X. Chen, R. C. Jin and H. J. Kim, *Journal of the American Chemical Society*, 2015, **137**, 14295-14304.

36. S. Das, A. Goswami, M. Hesari, J. F. Al-Sharab, E. Mikmekova, F. Maran and T. Asefa, *Small*, 2014, **10**, 1473-1478.
37. J. Fang, J. G. Li, B. Zhang, X. Yuan, H. Asakura, T. Tanaka, K. Teramura, J. P. Xie and N. Yan, *Nanoscale*, 2015, **7**, 6325-6333.
38. J. A. Lopez-Sanchez, N. Dimitratos, C. Hammond, G. L. Brett, L. Kesavan, S. White, P. Miedziak, R. Tiruvalam, R. L. Jenkins, A. F. Carley, D. Knight, C. J. Kiely and G. J. Hutchings, *Nature Chemistry*, 2011, **3**, 551-556.
39. B. Zhang, S. Kaziz, H. Li, M. G. Hevia, D. Wodka, C. Mazet, T. Burgi and N. Barrabes, *Journal of Physical Chemistry C*, 2015, **119**, 11193-11199.
40. E. Andrews, S. Katla, C. Kumar, M. Patterson, P. Sprunger and J. Flake, *Journal of the Electrochemical Society*, 2015, **162**, F1373-F1378.
41. J. A. Trindell, J. Clausmeyer and R. M. Crooks, *J Am Chem Soc*, 2017, **139**, 16161-16167.
42. J. P. Perdew, K. Burke and M. Ernzerhof, *Physical Review Letters*, 1996, **77**, 3865-3868.
43. J. VandeVondele and J. Hutter, *Journal of Chemical Physics*, 2007, **127**, 114105
44. S. Goedecker, M. Teter and J. Hutter, *Physical Review B*, 1996, **54**, 1703-1710.
45. J. VandeVondele, M. Krack, F. Mohamed, M. Parrinello, T. Chassaing and J. Hutter, *Computer Physics Communications*, 2005, **167**, 103-128.
46. Y. G. Wang, Y. Yoon, V. A. Glezakou, J. Li and R. Rousseau, *Journal of the American Chemical Society*, 2013, **135**, 10673-10683.
47. C. Y. Liu, Y. Z. Tan, S. S. Lin, H. Li, X. J. Wu, L. Li, Y. Pei and X. C. Zeng, *Journal of the American Chemical Society*, 2013, **135**, 2583-2595.
48. L. Ma, K. Laasonen and J. Akola, *Journal of Physical Chemistry C*, 2017, **121**, 10876-10886.
49. M. Prakash, K. Mathivon, D. M. Benoit, G. Chambaud and M. Hochlaf, *Physical Chemistry Chemical Physics*, 2014, **16**, 12503-12509.
50. Y. G. Wang, D. H. Mei, V. A. Glezakou, J. Li and R. Rousseau, *Nature Communications*, 2015, **6**.
51. M. Zhu, C. M. Aikens, F. J. Hollander, G. C. Schatz and R. Jin, *Journal of the American Chemical Society*, 2008, **130**, 5883-5885.
52. G. Li, H. Abroshan, C. Liu, S. Zhuo, Z. M. Li, Y. Xie, H. J. Kim, N. L. Ros and R. C. Jin, *Acs Nano*, 2016, **10**, 7998-8005.
53. J. K. Norskov, J. Rossmeisl, A. Logadottir, L. Lindqvist, J. R. Kitchin, T. Bligaard and H. Jonsson, *J. Phys. Chem. B*, 2004, **108**, 17886-17892.
54. J. B. Varley, H. A. Hansen, N. L. Ammitzboll, L. C. Grabow, A. A. Peterson, J. Rossmeisl and J. K. Norskov, *ACS Catal.*, 2013, **3**, 2640-2643.
55. D. F. Gao, H. Zhou, J. Wang, S. Miao, F. Yang, G. X. Wang, J. G. Wang and X. H. Bao, *Journal of the American Chemical Society*, 2015, **137**, 4288-4291.
56. S. A. Akhade, W. J. Luo, X. W. Nie, A. Asthagiri and M. J. Janik, *Catal. Sci. Technol.*, 2016, **6**, 1042-1053.
57. A. Venzo, S. Antonello, J. A. Gascon, I. Guryanov, R. D. Leapman, N. V. Perera, A. Sousa, M. Zamuner, A. Zanella and F. Maran, *Analytical Chemistry*, 2011, **83**, 6355-6362.
58. M. Z. Zhu, C. M. Aikens, M. P. Hendrich, R. Gupta, H. F. Qian, G. C. Schatz and R. C. Jin, *Journal of the American Chemical Society*, 2009, **131**, 2490-+.
59. M. Z. Zhu, W. T. Eckenhoff, T. Pintauer and R. C. Jin, *Journal of Physical Chemistry C*, 2008, **112**, 14221-14224.
60. G. Periyasamy, E. Durgun, J. Y. Raty and F. Remacle, *Journal of Physical Chemistry C*, 2010, **114**, 15941-15950.
61. J. A. Keith and E. A. Carter, *Journal of Chemical Theory and Computation*, 2012, **8**, 3187-3206.
62. K. Chan, C. Tsai, H. A. Hansen and J. K. Norskov, *Chemcatchem*, 2014, **6**, 1899-1905.
63. H. F. Qian, M. Y. Sfeir and R. C. Jin, *Journal of Physical Chemistry C*, 2010, **114**, 19935-19940.

64. J. Akola, M. Walter, R. L. Whetten, H. Häkkinen and H. Grönbeck, *Journal of the American Chemical Society*, 2008, **130**, 3756-3757.
65. X. Hong, K. R. Chan, C. Tsai and J. K. Norskov, *ACS Catal.*, 2016, **6**, 4428-4437.
66. D. Kim, C. L. Xie, N. Becknell, Y. Yu, M. Karamad, K. Chan, E. J. Crumlin, J. K. Norskov and P. D. Yang, *Journal of the American Chemical Society*, 2017, **139**, 8329-8336.
67. M. R. Singh, E. L. Clark and A. T. Bell, *Physical Chemistry Chemical Physics*, 2015, **17**, 18924-18936.
68. S. Zhao, R. X. Jin, Y. B. Song, H. Zhang, S. D. House, J. C. Yang and R. C. Jin, *Small*, 2017, **13**, 7.
69. S. Chretien, S. K. Buratto and H. Metiu, *Current Opinion in Solid State and Materials Science*, 2007, **11**, 62-75.
70. G. Mpourmpakis, A. N. Andriotis and D. G. Vlachos, *Nano Letters*, 2010, **10**, 1041-1045.
71. C. Shi, K. Chan, J. S. Yoo and J. K. Norskov, *Org. Process Res. Dev.*, 2016, **20**, 1424-1430.
72. X. W. Nie, W. J. Luo, M. J. Janik and A. Asthagiri, *Journal of Catalysis*, 2014, **312**, 108-122.

This work reveals the mechanism of CO_2 electrochemical reduction on ligand-protected Au nanoclusters and catalytic sites responsible for increased selectivity towards CO.